DOI: 10.1002/chem.200701305

Rapid Cooling Experiments and Use of an Anionic Nuclear Probe to Sense the Spin Transition of the 1D Coordination Polymers $[Fe(NH_2trz)_3]SnF_6 \cdot n\,H_2O$ (NH_2trz = 4-amino-1,2,4-triazole)

Yann Garcia,*[a] Vadim Ksenofontov,[b] Sophie Mentior,[a] Marinela M. Dîrtu,[a] Christine Gieck,[c] Ashis Bhatthacharjee,[b] and Philipp Gütlich*[b]

Dedicated to the memory of our friend Dr. Sergey Reiman

Abstract: $[Fe(NH_2trz)_3]SnF_6 \cdot n\,H_2O$ (NH_2trz = 4-amino-1,2,4-triazole; $n = 1$ (**1**), $n = 0.5$ (**2**)) are new 1D spin-crossover coordination polymers. Compound **2** exhibits an incomplete spin transition centred at around 210 K with a thermal hysteresis loop approximately 16 K wide. The spin transition of **2** was detected by the Mössbauer resonance of the ^{119}Sn atom in the SnF_6^{2-} anion primarily on the basis of the evolution of its local distortion. Rapid-cooling ^{57}Fe Mössbauer and superconducting quantum interference device experiments allow dramatic widening of the hysteresis width of **2** from 16 K up to 82 K and also shift the spin-transition curve into the room temperature region. This unusual behaviour of quenched samples on warming is attributed to activation of the molecular motion of the anions from a frozen distorted form towards a regular form at temperatures well above approximately 210 K. Potential applications of this new family of materials are discussed.

Keywords: cooperative phenomena · coordination polymers · lattice dynamics · Moessbauer spectroscopy · spin transition

Introduction

The fast developments in advanced electronic technology call for new compounds showing bistability behaviour on the nanometer scale.[1,2] Spin-transition (ST) molecular materials belong to an appealing class of switchable coordination compounds with spin states that can be reversibly triggered by temperature, pressure or electromagnetic radiation.[3,4] In this context, the reversible thermochromic ST of 1D Fe^{II} chain compounds with 4-substituted 1,2,4-triazole ligands that occurs around room temperature has been thoroughly investigated[5] with potential applications in mind (e.g., thermal displays, memory devices and sensors).[6,7] Because these materials of general formula $[Fe(4\text{-}(R)\text{-}1,2,4\text{-triazole})_3](anion)_2 \cdot n\,H_2O$ hardly crystallise, their polymeric nature was deduced by extended X-ray absorption fine structure (EXAFS) analysis at the Fe K-edge[8–10] and later confirmed by single-crystal X-ray analyses of a few Cu^{II} analogues.[9c,e,11,12] These compounds are made up of linear chains in which the adjacent Fe^{II} ions are linked by three N_1,N_2-1,2,4-triazole bridges (Figure 1). Non-coordinated species, such as solvent and/or counteranions, are located between the cationic chains. Most of these materials exhibit an abrupt ST with hysteresis loops 2 to 20 K wide that is accompanied by a pronounced thermochromic effect; these are characteristics that are suit for several potential applications.[6,7] Such cooperative ST behaviour is no longer ob-

[a] Prof. Dr. Y. Garcia, S. Mentior, M. M. Dîrtu
Unité de Chimie des Matériaux Inorganiques et Organiques
Département de Chimie
Université Catholique de Louvain, Place L.
Pasteur 1, 1348 Louvain-la-Neuve (Belgium)
Fax:(+32) 1047-2330
E-mail: yann.garcia@uclouvain.be

[b] Dr. V. Ksenofontov, Dr. A. Bhatthacharjee, Prof. Dr. P. Gütlich
Institut für Anorganische Chemie und Analytische Chemie
Universität Mainz
Staudingerweg 9, 55099 Mainz (Germany).
Fax:(+49) 6131-3922990
E-mail: guetlich@uni-mainz.de

[c] Dr. C. Gieck
Dipartimento di Scienze e Tecnologie Avanzate—Università del Piemonte Orientale "A. Avogadro"
Via Bellini 25/G,15100 Alessandria (Italy)

Supporting information for this article is available on the WWW under http://www.chemeurj.org/ or from the author.

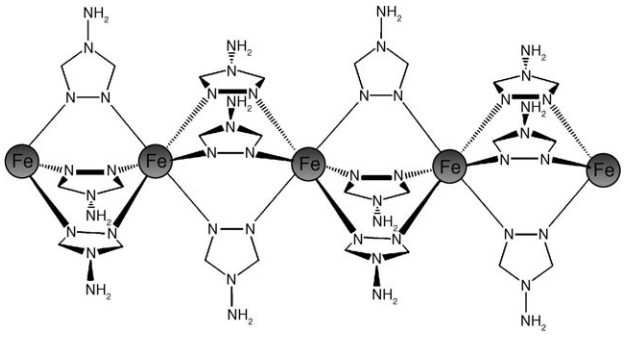

Figure 1. Schematic side-view of the polymeric chain structure of $[Fe(NH_2trz)_3]^{2+}$.[44]

served for chain compounds with bulky substituents on the 4-position of the triazole.[13–15]

$[Fe(Htrz)_2trz](BF_4)$ (Htrz = 4H-1,2,4-triazole; trz = 1,2,4-triazolato)[16,17] and $[Fe(NH_2trz)_3](NO_3)_2$ (NH_2trz = 4-amino-1,2,4-triazole)[18] are important examples of this family of materials because they exhibit a hysteretic ST ≈ 40[17] and ≈ 35 K,[18,19] wide, respectively. A structural modification from a linear conformation in the low-spin (LS) state to a zigzag one in the high-spin (HS) state was first proposed to account for the absence of long-range ordering in X-ray absorption experiments (EXAFS, wide-angle X-ray scattering (WAXS)) in the HS state for these materials.[9a–b,20] ESR measurements of the diluted sample $[Fe_{0.9}Cu_{0.1}(Htrz)_2trz](BF_4)$ showed systematic rhombic distortion in the HS state,[21] thus supporting the zigzag structural hypothesis that could have satisfactorily accounted for the observed hysteresis of the non-doped Fe^{II} ST derivative.[17] This hypothesis was, however, later rejected on the basis of more precise and comprehensive EXAFS measurements that unambiguously demonstrated the linearity conservation of the chains in the diamagnetic and paramagnetic states.[9e]

Abstract in French: *$[Fe(NH_2trz)_3]SnF_6 \cdot n H_2O$ (NH_2trz = 4-amino-1,2,4-triazole; n = 1 (**1**), n = 0.5 (**2**)) sont de nouveaux polymères de coordination 1D à transition de spin. Le composé **2** présente une transition incomplète centrée à ≈ 210 K avec une boucle d'hystérèse large de ≈ 16 K. La transition de spin de **2** a été sondée par résonance Mössbauer de l'atome d'^{119}Sn de l'anion SnF_6^{2-}, en particulier grâce à l'évolution de sa distorsion locale. Des cycles de refroidissements rapides et chauffage lent suivis par spectroscopie Mössbauer du ^{57}Fe et mesures SQUID ont permis d'élargir remarquablement la largeur de l'hystérèse de **2** passant de ≈ 16 K à ≈ 82 K, et de déplacer la courbe de transition de spin dans la région de la température ambiante. Ce comportement inhabituel au chauffage pour les échantillons piégés a été attribué à l'activation thermique du mouvement moléculaire des anions; d'une forme gelée distordue vers une forme régulière à des températures bien au-delà de ≈ 210 K. Les applications potentielles de cette nouvelle famille de matériaux sont discutées.*

Given that no crystallographic phase transition accompanying the ST was observed for $[Fe(Htrz)_2trz](BF_4)$ by variable-temperature synchrotron X-ray powder diffraction experiments,[22] the origin of the hysteresis loop was primarily attributed to the propagation of short-range elastic cooperative effects through the rigid 1,2,4-triazole bridge between spin-changing Fe^{II} sites (Figure 1).[5] These interactions were probed by metal dilution studies of $[Fe_{1-x}Cu_x(Htrz)_2trz](BF_4)$[21] and $[Fe_{1-x}M_x(NH_2trz)_3](NO_3)_2$ (M^{II} = Zn, Ni, Mn, Cu),[23–26] in which a systematic decrease in the steepness of the ST was observed, as expected for the accompanying decrease in elastic interactions (short and long range) within the polymeric chain. Little is known, however, about the role of long-range elastic interactions in the crystal lattice of these materials that are believed to play a key role in the propagation of cooperative effects associated with the ST of individual chains throughout the whole network. These effects could be mediated through non-coordinated species, such as the anions or solvent molecules, but this role has not yet been experimentally proven. However, the influence of the nature and the geometry of the counteranion is known to affect the ST temperature, $T_{1/2}$, of these materials. Indeed, the insertion of spherical counteranions, such as halogen anions, leads to a higher $T_{1/2}$ compared with bulkier anions, such as BF_4^- and ClO_4^-.[27,28] Solvent effects with the same consequences on the spin state were also found for the chain $[Fe(hyetrz)_3](3\text{-nitrophenylsulfonate})_2 \cdot n$ Solv (hyetrz = 4–2′-hydroxyethyl-1,2,4-triazole; Solv = H_2O, MeOH, DMF, DMA).[29]

In the present work, an internal anionic probe was successfully implanted in the crystal lattice of the 1D chain compounds $[Fe(NH_2trz)_3]SnF_6 \cdot n H_2O$ with the aim of sensing supramolecular cooperative effects associated with the spin transition. These new materials, including SnF_6^{2-} as counteranions, offer a new opportunity to probe locally the thermally induced ST by means of two Mössbauer isotopes located within the chain (^{57}Fe) and in the anionic sublattice (^{119}Sn). We also report the influence of anionic sublattice dynamics on ST behaviour, which is sensed by rapid-cooling Mössbauer spectroscopy and superconducting quantum interference device (SQUID) experiments. Potential applications of these materials are also briefly discussed.

Results

Syntheses: A monohydrate complex was precipitated as a white powder by mixing warm solutions of $[Fe(H_2O)_6]SnF_6$ and NH_2trz (1:3) in methanol; the precipitate was washed with methanol and dried in air. Elementary analyses and thermogravimetric measurements confirmed the composition as $[Fe(NH_2trz)_3]SnF_6 \cdot H_2O$ (**1**; Figure 2). The white colour of the precipitate is characteristic of the HS state of the Fe^{II} centres. Indeed, the absence of charge-transfer transitions in the visible range allows an easy identification of the spin state because the spin-allowed lowest-energy d–d transition, $^5T_{2g} \rightarrow {}^5E_g$, for the HS Fe^{II} ions occurs in the near-

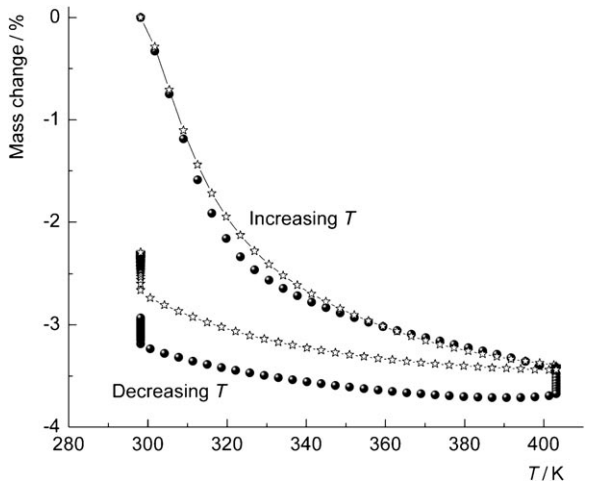

Figure 2. Thermogravimetric analysis (recorded at 1 K min^{-1}) for **1** (☆) and **2** (●) over the temperature range 298 to 403 K on warming and cooling. A standby period of 30 min at 403 K was included for **2** in its temperature programme.

IR region ($\tilde{\nu} \approx 11\,900$ cm^{-1}). The precipitate obtained during the synthesis of **1** was pumped under vacuum at 50 °C for 30 min. This annealing process afforded [Fe(NH$_2$trz)$_3$]SnF$_6$·0.5 H$_2$O (**2**) and its degree of hydration was confirmed by TGA measurements (Figure 2). The reproducibility of this preparation method under the very same conditions was checked twice. On standing in air for a long period, a **2**→**1** transformation slowly occurs (as confirmed by thermogravimetric measurements), but the degree of hydration of **2** can be maintained provided the sample is kept under a nitrogen atmosphere. Attempts to isolate the fully dehydrated material **3** from **1** or **2** under ambient conditions failed because the dehydrated materials slowly reabsorb water molecules in ambient air, as seen in Figure 2, both on cooling from 403 K and on standing at room temperature.

Compounds **1** and **2** exhibit reversible thermochromism to deep purple on quenching of the sample in liquid nitrogen. This colour change is a signature of a thermally induced spin-crossover (SCO) phenomenon. Indeed, this purple colour is due to the $^1A_{1g} \rightarrow {}^1T_{1g}$ d–d transition of LS Fe^{II} ions, which occurs at ≈520 nm.[6a] The nature of the SCO behaviour in these samples on cooling and re-warming has been tracked by using several techniques (see below).

Infrared spectroscopy: Compounds **1** and **2** have essentially identical IR spectra at room temperature. The ring stretch found at $\tilde{\nu} = 1544$ cm^{-1}, $\delta(NH_2)$ at ≈1630 cm^{-1} and the exocyclic N–N bond stretch at ≈1216 cm^{-1} exactly correspond to the vibrations reported in the spectroscopic study of [Cu(NH$_2$trz)$_3$](ClO$_4$)$_2$·0.5 H$_2$O, a Cu^{II} complex containing triple N_1,N_2-triazole bridges whose 1D character was recognised.[30] This indicates that coordination to the Fe^{II} ion takes place exclusively through the azole ring.[30] The absence of noticeable splitting for the IR-active vibration ν_3 for SnF_6^{2-} observed at 555 cm^{-1} calls for a symmetric octahedron (O_h).[31]

X-ray powder diffraction: Compounds **1** and **2** are isomorphous as deduced by comparison of the X-ray powder diffraction patterns recorded at room temperature (Figure S1 in the Supporting Information). Thus, slight variances in the water content does not noticeably modify the structural organisation of these materials.

Mössbauer spectroscopy: The present Fe^{II} compounds are stable to oxidation because no ferric species were detected in the ^{57}Fe Mössbauer spectra of **2**. The Mössbauer parameters, reported in Table 1, are consistent with other 1D Fe^{II} coordination polymers with the NH$_2$trz ligand.[32] The ^{119}Sn Mössbauer spectrum of **2** recorded at 300 K shows a single line with an isomer shift at $\delta \approx -0.3$ mm s^{-1} (relative to the source ^{119}Sn(CaSnO$_3$)), which confirms the Sn^{IV} oxidation state for the anion. This low isomer shift fits very well with the value obtained at 300 K for CuSnF$_6$ ($\delta = -0.35(5)$ mm s^{-1}),[33] but is less negative than those found for the hydrated salts at 300 K ([Fe(H$_2$O)$_6$]SnF$_6$: $\delta = -0.437$ mm s^{-1}[34] and CuSnF$_6$·4 H$_2$O: $\delta = -0.46(1)$ mm s^{-1}[33]). This behaviour suggests that the SnF_6^{2-} octahedron in **2** is not hydrogen bonded to water molecules. Indeed, in the crystal structure of [Fe(H$_2$O)$_6$]SnF$_6$, the SnF_6^{2-} octahedron is hydrogen bonded to the coordinated water molecules,[35] which reduces the donation of electrons from the fluorine, and thus, decreases the s-electron density at the Sn atom thereby shifting the isomer shift to a more negative value. The absence of quadrupole splitting at 300 K for **2** is consistent with the IR observation described above that suggested a regular octahedral coordination sphere.

Study of the spin transition in [Fe(NH$_2$trz)$_3$]SnF$_6$·*n*H$_2$O: We present the study of the thermally induced ST of [Fe(NH$_2$trz)$_3$]SnF$_6$·*n* H$_2$O ($n = 0$–1.5) by slow cooling (SC) and warming below room temperature by means of SQUID magnetometry, Mössbauer spectroscopy (^{57}Fe, ^{119}Sn), X-ray powder diffraction and differential scanning calorimetry (DSC).

SQUID magnetometry: The temperature dependence of the molar magnetic susceptibility of **1**, **2** and **3** (fully dehydrated compound, $n = 0$), on cooling and warming over the temperature range 300 to 5 K, is displayed in Figure 3 in the form of a $\chi_M T$ versus T plot, in which χ_M is the molar magnetic susceptibility. At room temperature, $\chi_M T$ is equal to 3.19 cm^3 mol^{-1} K for **1**, which corresponds to a major fraction of Fe^{II} ions in the HS state, presumably some Fe^{II} ions are also in the LS state. As T is lowered, $\chi_M T$ first decreases very slowly to 225 K and then rapidly to 150 K. Below this temperature, $\chi_M T$ decreases very slowly and shows a plateau with a value of 0.56 cm^3 mol^{-1} K at 50 K, indicating an incomplete HS→LS transition. The slow fall of $\chi_M T$ below 25 K is attributed to the effect of zero-field splitting of the remaining HS Fe^{II} ions, and the preferred Boltzmann population of the lowest levels with decreasing temperatures. As the temperature is increased, $\chi_M T$ follows the same pathway as that observed when cooling except in the range of 150 to

Table 1. Overview of the ^{57}Fe Mössbauer parameters for **2**.

T[a] [K]	δ[b] [mm s^{-1}]	ΔE_Q[c] [mm s^{-1}]	Γ[d] [mm s^{-1}]	Relative area [%]	Sites
80[e]	1.16(1)	3.38(1)	0.30(1)	15.5(6)	HS
	0.52(1)	0.28(2)	0.28(1)	84.5(4)	LS
120↑	1.15(5)	3.34(1)	0.32(1)	16.1(6)	HS
	0.52(1)	0.27(1)	0.28(1)	83.9(4)	LS
210↑	1.10(1)	3.13(2)	0.36(2)	9.5(6)	HS
	0.49(1)	0.25(1)	0.26(1)	90.5(3)	LS
230↑	1.10(1)	3.08(2)	0.38(2)	9.9(8)	HS
	0.48(1)	0.24(1)	0.26(1)	90.1(5)	LS
250↑	1.08(1)	2.99(2)	0.38(2)	10.5(9)	HS
	0.47(1)	0.23(1)	0.26(1)	89.5(5)	LS
270↑	1.06(3)	2.87(2)	0.30(1)	35.4(9)	HS
	0.45(3)	0.23(1)	0.26(1)	64.6(6)	LS
290↑	1.05(1)	2.79(3)	0.26(1)	92.6(1)	HS
	0.45[d]	0.22[d]	0.6(1)	7.4(2)	LS
300	1.04(4)	2.75(1)	0.26(1)	100	HS
270↓	1.06(1)	2.87(2)	0.28(1)	96.3(1)	HS
	0.45[d]	0.3[d]	0.6(3)	3.7(2)	LS
250↓	1.08(1)	2.95(2)	0.28(1)	93.9(1)	HS
	0.42(5)	0	0.6(1)	6.1(2)	LS
230↓	1.08(1)	3.03(2)	0.28(1)	91.3(9)	HS
	0.46(2)	0.22(5)	0.36(4)	8.7(9)	LS
210↓	1.10(1)	3.10(2)	0.28(1)	80.5(8)	HS
	0.49(1)	0.25(1)	0.30(1)	19.5(6)	LS
190↓	1.11(2)	3.16(2)	0.28(1)	42.9(1)	HS
	0.50(1)	0.28(1)	0.26(1)	57.1(4)	LS
170↓	1.12(2)	3.21(2)	0.30(1)	35.0(1)	HS
	0.51(1)	0.287(2)	0.26(1)	65.0(4)	LS
120↓	1.15(3)	3.33(1)	0.30(1)	23.0(7)	HS
	0.52(1)	0.30(2)	0.28(1)	77.0(1)	LS
82↓	1.16(4)	3.38(8)	0.32(1)	20.6(6)	HS
	0.53(1)	0.31(2)	0.28(1)	79.4(4)	LS
120↑	1.15(1)	3.34(1)	0.32(1)	23.3(4)	HS
	0.52(1)	0.30(1)	0.28(1)	76.7(3)	LS
170↑	1.12(2)	3.22(2)	0.30(1)	32.7(6)	HS
	0.51(1)	0.28(1)	0.26(1)	67.3(4)	LS
190↑	1.11(2)	3.17(2)	0.30(1)	37.8(7)	HS
	0.50(1)	0.28(1)	0.26(1)	62.2(4)	LS
210↑	1.10(2)	3.11(1)	0.30(1)	48.6(7)	HS
	0.49(2)	0.27(1)	0.26(1)	51.4(5)	LS
230↑	1.10(1)	3.05(1)	0.28(1)	75.6(8)	HS
	0.48(1)	0.25(1)	0.28(1)	24.4(6)	LS
250↑	1.08(1)	2.98(1)	0.28(1)	89.8(1)	HS
	0.46(2)	0.22(2)	0.34(1)	10.2(1)	LS
270↑	1.06(1)	2.89(1)	0.26(1)	95.2(8)	HS
	0.39(4)	0	0.6(2)	4.8(1)	LS
300	1.05(2)	2.78(1)	0.26(1)	97.1(2)	HS
	0.19(1)	0.4(1)	0.2(1)	2.9(1)	LS
80[e]	1.16(4)	3.40(1)	0.34(1)	18.7(6)	HS
	0.53(1)	0.32(1)	0.28(1)	81.3(4)	LS
120↑	1.15(4)	3.37(1)	0.32(1)	19.3(6)	HS
	0.53(1)	0.31(1)	0.28(1)	80.7(4)	LS
210↑	1.11(2)	3.18(1)	0.28(1)	36.3(7)	HS
	0.50(1)	0.28(2)	0.26(1)	63.7(5)	LS
230↑	1.09(1)	3.04(3)	0.28(1)	87.3(9)	HS
	0.47(1)	0.24(2)	0.30(2)	12.6(8)	LS
250↑	1.08(1)	3.01(2)	0.28(1)	90.4(8)	HS
	0.46(1)	0.25(2)	0.32(2)	9.6(6)	LS
270↑	1.06(1)	2.93(3)	0.28(1)	93.0(1)	HS
	0.14(4)	0.66(7)	0.36(5)	7.0(2)	LS
300	1.05(2)	2.79(1)	0.26(1)	96.6(2)	HS
	0.2(1)	0	0.4(5)	3.4(3)	LS
80[e]	1.16(5)	3.40(1)	0.32(1)	18.8(7)	HS
	0.53(1)	0.32(1)	0.28(1)	81.2(4)	LS
120↑	1.15(4)	3.36(1)	0.32(1)	19.0(1)	HS
	0.53(1)	0.31(1)	0.28(1)	81.0(4)	LS

Table 1. (Continued)

T[a] [K]	δ[b] [mm s^{-1}]	ΔE_Q[c] [mm s^{-1}]	Γ[d] [mm s^{-1}]	Relative area [%]	Sites
210↑	1.10(1)	3.12(2)	0.30(1)	49.5(4)	HS
	0.50(1)	0.27(2)	0.26(1)	50.5(3)	LS
230↑	1.10(1)	3.09(3)	0.28(1)	63.3(8)	HS
	0.49(1)	0.27(1)	0.26(1)	36.7(6)	LS
250↑	1.08(1)	2.98(1)	0.28(1)	92.8(1)	HS
	0.41(4)	0	0.4(2)	7.2(2)	LS
270↑	1.06(1)	2.88(1)	0.26(1)	92.0(1)	HS
	0	0	0.46(8)	8.0(2)	LS
300	1.04(2)	2.77(1)	0.26(1)	95.6(2)	HS
	0.3(2)	0.2(2)	0.8(6)	4.4(4)	LS

[a] ↑ indicates warming and ↓ indicates cooling. [b] δ = isomer shift relative to α-iron. [c] ΔE_Q = quadrupole splitting. [d] Γ = width at half maximum. [e] Values obtained after rapid cooling.

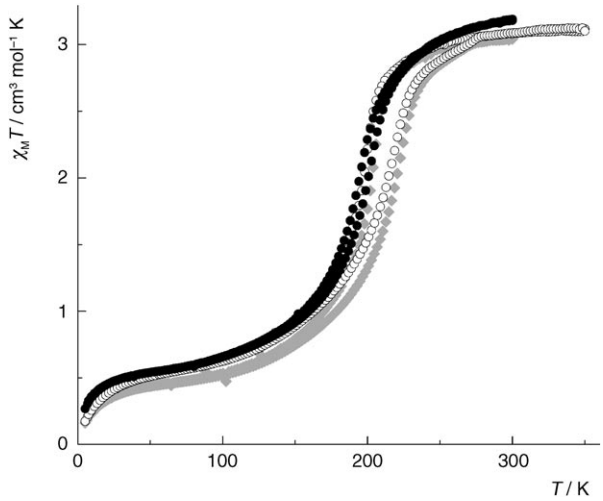

Figure 3. Temperature dependence of $\chi_M T$ on cooling and warming for $[Fe(NH_2trz)_3]SnF_6 \cdot n H_2O$ ($n=1$ (**1**, ●), $n=0.5$ (**2**, ◆) and $n=0$ (**3**, ○).

225 K, which indicates a hysteresis loop ≈7 K wide centred at 190 K. The transition temperatures (the temperatures at which 50% of active LS and HS molecules are present) in the cooling and warming modes, respectively, are $T_{1/2}\downarrow =$ 193 K and $T_{1/2}\uparrow = 200$ K. This hysteresis is retained over successive cooling and heating thermal cycles, provided the temperature does not exceed 300 K to avoid dehydration of the sample, which is shown to occur by thermogravimetric measurements (Figure 2). The magnetic properties of hemihydrate **2** were also investigated by SQUID measurements. $\chi_M T$ is constant at 3.04 cm^3 mol^{-1} K over the temperature range 300 to 250 K, which suggests the presence of a fraction of LS Fe^{II} ions that were detected by Mössbauer spectroscopy (Figure 4). The shape of the ST curve is similar to that of **1**, however, it reaches lower $\chi_M T$ values at 50 K (0.42 cm^3 mol^{-1} K), which indicates a more complete ST. The ST is shifted upwards to higher temperatures and a larger width of ≈16 K ($T_{1/2}\downarrow = 201$ K and $T_{1/2}\uparrow = 217$ K) is observed.

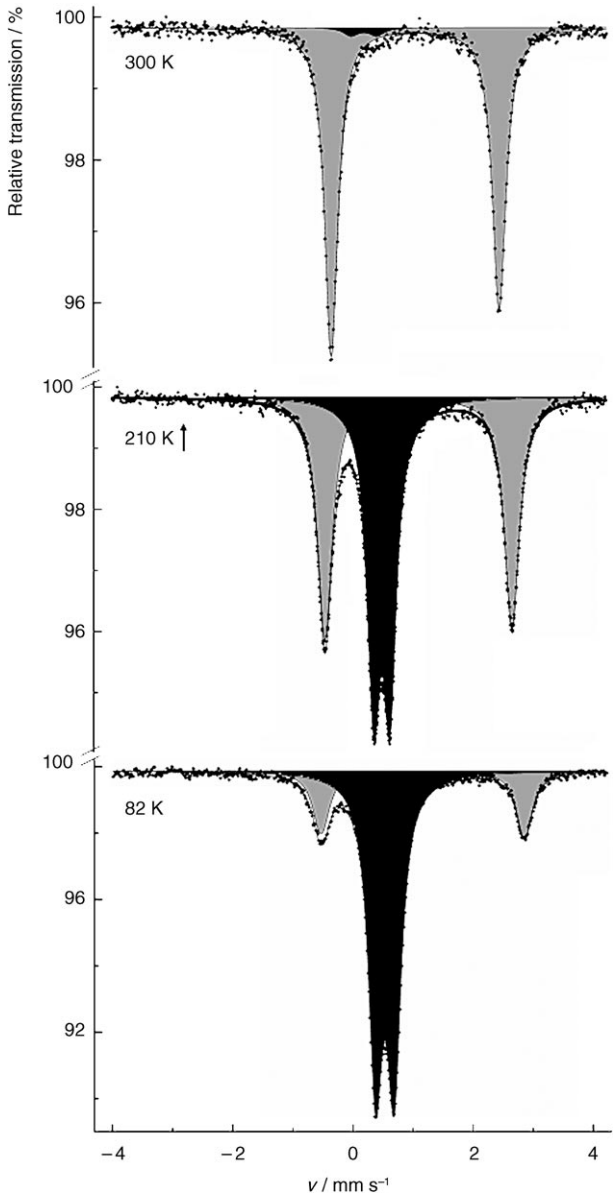

Figure 4. ^{57}Fe Mössbauer spectra of **2** at selected temperatures on warming after slowly cooling the sample to 82 K. The light grey and black signals refer to HS and LS Fe^{II} ions, respectively.

A fresh sample of **2** was loaded in the SQUID cavity at 300 K and the temperature was raised to 350 K. The magnetisation data was subsequently recorded, on cooling and warming, over the temperature range 350 to 5 K in increments of 2 K. This in situ thermal treatment allows recording of the magnetic properties of the fully dehydrated sample of $[Fe(NH_2trz)_3]SnF_6$ (**3**). Indeed, on warming the sample from 298 to 350 K at 1 K min^{-1}, only 0.2 water molecules remain in the sample, as determined by complementary TGA measurements (Figure 2). Because the material is first warmed from 300 to 350 K within the SQUID cavity, then slowly cooled to 293 K and has to stabilise its temperature at each 2 K interval to allow data to be recorded, we can be confident that full dehydration is reached with this process. The shape of the ST curve is preserved compared to **2**, but the ST is shifted slightly downwards ($T_{1/2}\downarrow = 197$ K and $T_{1/2}\uparrow = 210$ K).

^{57}Fe Mössbauer spectroscopy: Selected Mössbauer spectra of **2** recorded in the heating mode after cooling the sample slowly from room temperature are displayed in Figure 4. At 82 K, the spectrum consists of two quadrupole doublets of different resonance area fractions. The major quadrupole doublet with isomer shift $\delta = 0.53(1)$ mm s^{-1} and quadrupole splitting of $\Delta E_Q = 0.31(2)$ mm s^{-1} correspond to the LS state of Fe^{II}. The presence of the quadrupole splitting in this case stems from a so-called lattice contribution to the electric field gradient and thus, reveals a distorted character for the LS octahedron as expected within a chain, in which constraints may not be negligible. Another doublet, corresponding to HS Fe^{II} ions of weaker population (20.6%), is also observed ($\delta = 1.16(4)$ mm s^{-1} and $\Delta E_Q = 3.38(8)$ mm s^{-1}). The presence of this doublet confirms the incomplete nature of the ST at 82 K as also found by SQUID magnetometry (Figure 3). It is likely that the incomplete character of the ST may stem from the terminal of chains of the FeN_6-type compound, which have a ligand field strength too weak to meet conditions for a thermally induced SCO to occur.[36] It is unlikely that end of chains of the FeN_3O_3-type with three terminally coordinated water molecules are responsible for the residual HS fraction. In this case, the quadrupole splitting would be expected to be much smaller than the actually observed value of 3.38 mm s^{-1} because the lattice contribution to the electric field gradient (EFG) arising from the mixed-ligand coordination sphere FeN_3O_3 is expected to be larger than that from a FeN_6 entity and owing to the known opposite sign to that of the valence electron contribution which reduces the total EFG more than in the case of FeN_6. This is observed for the terminal Fe^{II} ions of trinuclear $[Fe_3(4\text{-ethyl-}1,2,4\text{-triazole})_6(H_2O)_6](CF_3SO_3)_6$ with $\Delta E_Q = 2.51$ mm s^{-1} at 77 K.[37] In other cases, however, the quadrupole splitting for external iron(II) ions can be larger than for an FeN_6 octahedron, as determined by the ^{57}Fe Mössbauer studies of structurally characterised trinuclear complexes of $[Fe_3(4\text{-isopropyl-}1,2,4\text{-triazole})_6(H_2O)_6](Tos)_6{\cdot}2H_2O$[38] (Tos = *p*-toluenesulfonate) and $[Fe_3(4\text{-}2'\text{-hydroxyethyl-}1,2,4\text{-triazole})_6(H_2O)_6](CF_3SO_3)_6$.[39] This situation is explained by the negligible lattice contribution to the EFG from the local FeN_3O_3 *fac*-isomer configuration.[40] In the present case, the observed quadrupole splitting of 3.38 mm s^{-1} is close to that expected for Fe^{II} HS compounds with little or no lattice contribution to the EFG. We believe that the terminal entities of the chains only consist of FeN_6 octahedra because a unique site was observed on varying the temperature. The presence of two terminally coordinated water molecules that may not be detected by Mössbauer spectroscopy[41] should, however, also be considered. On warming to 210 K, the intensity of the HS doublet increases at the expense of that of the LS doublet, which confirms a thermally induced LS→HS conversion for a single Fe^{II} site. At 300 K, the spec-

trum clearly shows a major signal corresponding to HS Fe^{II} ions, with a remaining weaker fraction of LS ions (3.0%), which had to be taken into account for the reliability of the fitting procedure. This confirms the incomplete character of the ST at room temperature, as suggested in the SQUID investigation. The asymmetry of the quadrupole doublet corresponding to HS Fe^{II} ions is attributed to a texture effect. The ST curve, deduced from ^{57}Fe Mössbauer spectroscopy considering equal Lamb–Mössbauer factors for the LS and HS Fe^{II} ions, closely resembles that deduced from magnetic measurements (Figure 11 in the ST range) with $T_{1/2}\uparrow = 216$ K and $T_{1/2}\downarrow = 196$ K.

X-ray powder diffraction: X-ray diffraction patterns of **2** have been recorded on cooling and warming over the temperature range 270 K to 100 K. Figure 5 shows three typical

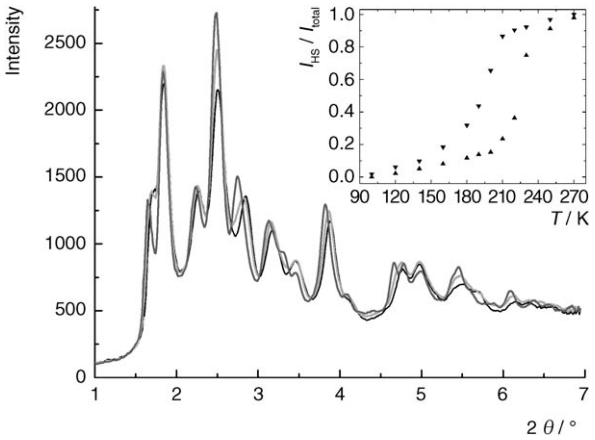

Figure 5. X-ray diffraction patterns of **2** at 100 (——), 180 (——) and 270 K (——). The inset shows the temperature dependence of the relative intensity of the HS phase I_{HS}/I_{Total} peak at $2\theta \approx 2.5°$. The data were recorded on cooling and warming.

diffraction patterns. The diffraction patterns are essentially similar and suggest the absence of a crystallographic phase transition. However, a decrease in the intensity of some peaks is observed, whereas other peaks grow in intensity as shown by comparing the patterns at 270 and 100 K. This behaviour is correlated to the spin-state crossover that occurs at around 200 K, as tracked by SQUID and ^{57}Fe Mössbauer spectroscopy. It is evident that at the intermediate temperature of 180 K, the spectrum shows a superposition of the patterns for the HS and LS phases with a temperature-dependent intensity. On this basis, we selected the intensity of a peak at $2\theta \approx 2.5°$ as a marker to track the ST and the hysteresis loop whose dependence is shown in the inset to Figure 5. The transition temperatures of $T_{1/2}\uparrow \approx 197$ K and $T_{1/2}\downarrow \approx 224$ K were derived. These values are in good agreement with those obtained by Mössbauer spectroscopy. The transition curve is very gradual and as such points to the presence of a non-first-order phase transition.

Calorimetric measurements: Compounds **1** and **2** were investigated over the temperature range 98 to 298 K on cooling and warming at 5 K min^{-1}. Transition temperatures as well as enthalpy and entropy values are gathered in Table 2. The DSC response for **2** is given as an example in Figure 6. Exo-

Table 2. Thermodynamic parameters and transition temperatures for **1** and **2**.

	$T_{max}\downarrow$ [K]	$T_{max}\uparrow$ [K]	ΔH [kJ mol^{-1}]	ΔS [J mol^{-1} K^{-1}]	ΔS_{vib} [J mol^{-1} K^{-1}]
1	207	–	7	34	20.6
2	225	203	6.9	34	20.6

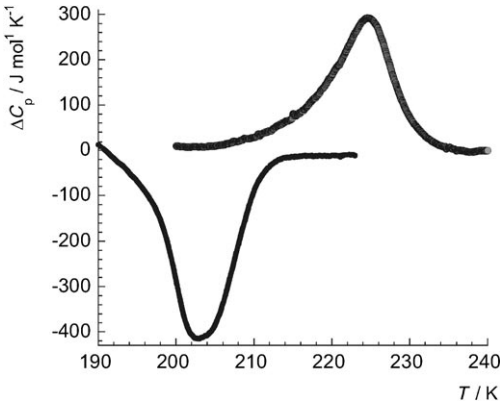

Figure 6. DSC measurements of **2** in the 190 to 240 K temperature range. The cooling and warming modes are in black and grey, respectively.

thermic and endothermic peaks are observed at $T_{max} \approx 203$ and 225 K, respectively, thus clearly confirming the presence of a hysteresis loop. These peaks are obviously related to the ST detected by Mössbauer, magnetic and XRPD studies, and probably may call for the presence of a first-order phase transition. The enthalpy and entropy variations have been evaluated as $\Delta H = 6.9$ kJ mol^{-1} and $\Delta S = 34$ J mol^{-1} K^{-1}, respectively, by considering the transition of the active Fe^{II} ions (76.5%) and the fraction of Fe spins undergoing the SCO in this temperature range (40%), as deduced from Mössbauer measurements. The experimentally measured entropy variation can be accounted for by an electronic contribution, $R \times \ln 5 = 13.4$ J mol^{-1} K^{-1}, and a vibrational contribution (20.6 J mol^{-1} K^{-1}).[3] The presence of a structural phase transition accompanying the ST should dramatically increase the ΔS value, which is not observed here (Table 2).[3]

^{119}Sn Mössbauer spectroscopy: ^{119}Sn Mössbauer spectra were recorded by slow cooling and warming **2** over the temperature range 300 to 80 K followed by another cooling mode to 4.2 K to track any possible hysteresis loop. The ^{119}Sn Mössbauer parameters are given in Table 3. Figure 7 shows representative ^{119}Sn Mössbauer spectra recorded at 80 K. The

Table 3. Overview of the ^{119}Sn Mössbauer parameters for **2**.

T [K]	δ[a] [mm s^{-1}]	ΔE_Q[b] [mm s^{-1}]	$\Gamma/2$[c] [mm s^{-1}]	Relative area [%]
300	−0.37(6)	0	0.4(1)	100
230↓	−0.29(2)	0	0.55(3)	100
190↓	−0.29(3)	0	0.52(1)	100
130↓	−0.28(1)	0.28(2)	0.57(1)	100
80↓	−0.27(2)	0.34(2)	0.54(1)	100
130↑	−0.282(2)	0.29(2)	0.52(1)	100
190↑	−0.29(1)	0	0.52(1)	100
230↑	−0.30(1)	0	0.53(2)	100
260↑	−0.30(2)	0	0.49(4)	100
300	−0.29(6)	0	0.4(1)	100
210↓	−0.30(1)	0	0.50(1)	100
160↓	−0.29(1)	0.24(3)	0.49(1)	100
110↓	−0.28(2)	0.28(2)	0.53(1)	100
90↓	−0.28(2)	0.31(2)	0.54(1)	100
5↓	−0.26(1)	0.40(5)	0.61(2)	100
40↑	−0.27(1)	0.36(3)	0.59(1)	100
4.2↓	−0.26(1)	0.39(5)	0.62(2)	100

[a] δ = isomer shift relative to the source ^{119}Sn(CaSnO$_3$). [b] ΔE_Q = quadrupole splitting. [c] $\Gamma/2$ = half width at half maximum.

temperature variation of δ shown in Figure 8 reveals a linear increase on cooling that is attributed to a second-order Doppler shift. The normalised resonance area shown in Figure 9 clearly evidences two linear temperature domains of different slopes. Interestingly, a jump is found at around 190 K on cooling, a feature that is a clear signature of a phase transition. Indeed, such a jump is observed by ^{57}Fe Mössbauer spectroscopy while crossing the ST range. But contrary to Fe^{II} and Fe^{III} SCO compounds,[42,43] there is no change of effective mass expected with Sn, which leads to an accurate determination of the Debye temperature and characterises the rigidity of the Sn–F bonds. Nevertheless, this characteristic temperature is not expected to be dramatically modified by the spin-state crossover in the present case because the SnF_6^{2-} ions occupy lattice positions that are not in the close neighbourhood of the spin-changing iron ions. Interestingly, the appearance of ΔE_Q below 190 K was observed for **2** (see Figure 9, inset), which means that the anionic SnF_6^{2-} octahedron becomes distorted below this temperature and is regular above it. This observation satisfactorily matches the IR spectrum at 300 K, which suggested a regular octahedron. This overall behaviour reflects a phase transition at around 190 K that results from the spin-state change in individual chains, which was detected in the same temperature range by other physical methods.

Rapid cooling experiments: Rapid cooling (RC) experiments were performed, from room temperature to liquid nitrogen temperature, to investigate the possible dynamics of the SnF_6^{2-} ion in the crystal lattice of Fe^{II} chain compounds and to study their influence on the spin-state crossover. Compound **2** was selected for these experiments because it displays the widest hysteresis loop in the series.

^{57}Fe Mössbauer spectroscopy: Rapid cooling experiments were carried out on **2**. At 80 K, the spectrum shows a major quadrupole doublet ($\delta = 0.52(1)$ mm s^{-1}, $\Delta E_Q =$ 0.28(2) mm s^{-1}), which corresponds to LS Fe^{II} ions ($\approx$85 %), and another doublet of weaker intensity ($\approx$15 %), which corresponds to HS Fe^{II} ions ($\delta = 1.16(1)$ mm s^{-1}, $\Delta E_Q =$ 3.38(1) mm s^{-1}). These parameters nicely correspond to those recorded at 82 K on slow cooling (Figure 4), which confirms the absence of thermal trapping of a metastable HS state. Mössbauer spectra were then recorded on slow warming and cooling over the temperature range of 80 to 300 K, followed by slow warming to 300 K. The corresponding HS molar fraction (γ_{HS}) that was derived from the spectra is plotted in Figure 10. The compound mostly stays in the LS state up to 250 K. A slight decrease of γ_{HS} is observed over the temperature range 120 to 210 K. This decrease may be slightly overestimated owing to the somewhat

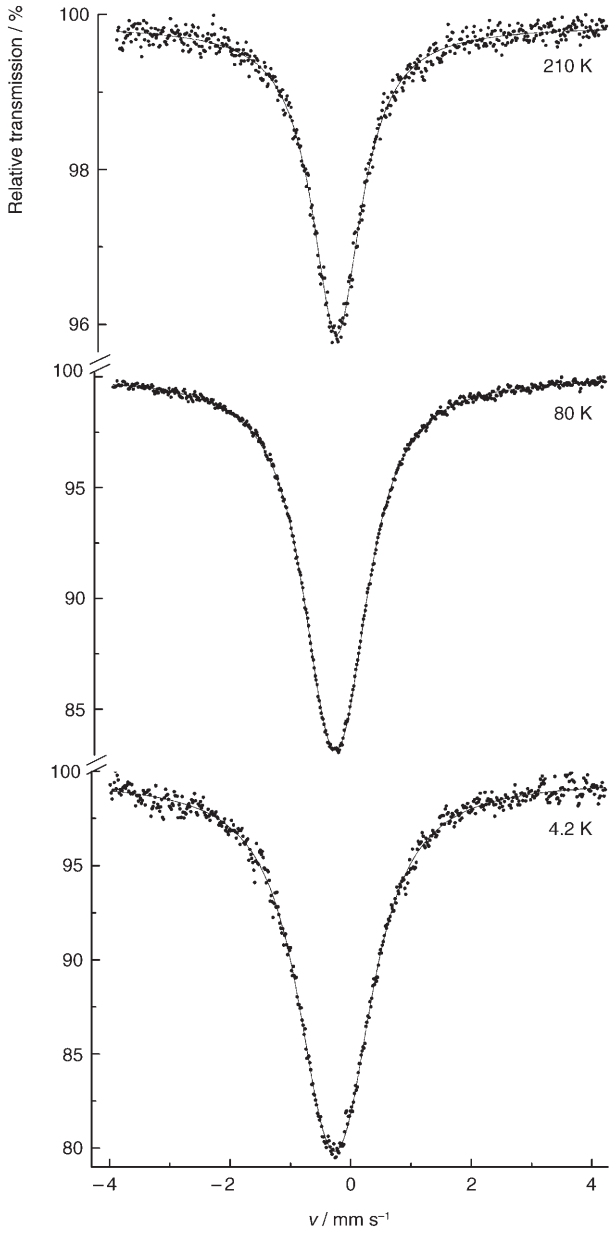

Figure 7. ^{119}Sn Mössbauer spectra of **2** at selected temperatures recorded on cooling from 300 K.

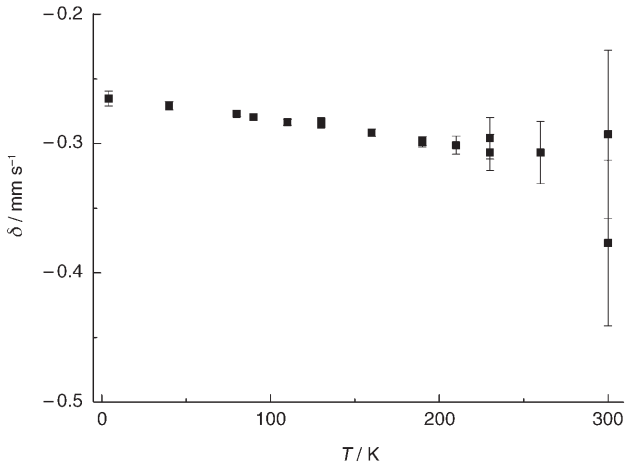

Figure 8. Temperature dependence of the isomer shift δ (relative to the source $^{119}Sn(CaSnO_3)$ of **2** over the temperature range 300 to 4.2 K on cooling and warming, as deduced from ^{119}Sn Mössbauer spectroscopy.

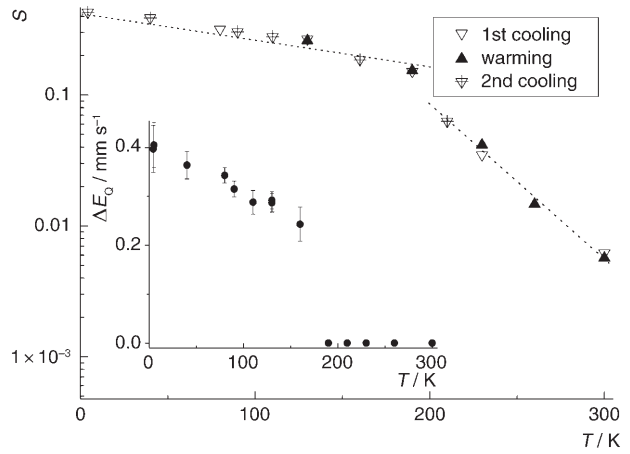

Figure 9. Temperature dependence of the normalised resonance area, *S*, with a logarithmic scale of **2** over the temperature range 300 to 4.2 K on cooling and warming, as deduced from ^{119}Sn Mössbauer spectroscopy. The inset shows the temperature dependence of the quadrupole splitting ΔE_Q over the same temperature range.

higher Debye–Waller factor of the LS Fe^{II} ions compared with the HS ions as a consequence of the stronger metal–ligand bonds and a more rigid lattice for the LS state. This effect is well known with Mössbauer spectroscopy on SCO complexes of iron, and the resulting uncertainty is estimated to be less than five percent. For comparison, the sample should have switched to the HS state at ≈200 K if the LS→HS conversion pathway had been followed without the RC procedure. We note that no relaxation occurs with time at these temperatures, in which the compound is in the LS state, because each Mössbauer spectrum was recorded for at least one day to reach an acceptable signal-to-noise ratio. Above 250 K, γ_{HS} sharply increases up to 300 K with values that correspond to the HS state. Upon cooling to 80 K, and slow warming, a ST behaviour similar to that found by SQUID measurements is observed (Figure 10).

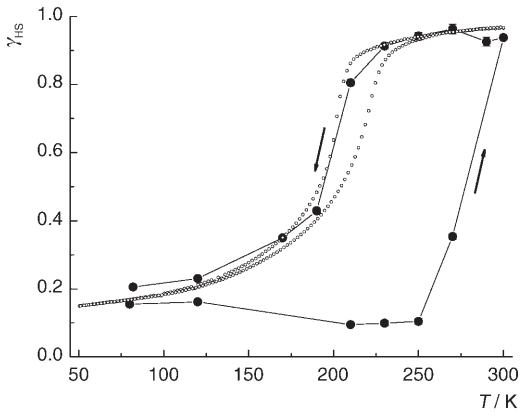

Figure 10. Temperature dependence of the molar fraction of HS molecules, γ_{HS}, as deduced from ^{57}Fe Mössbauer measurements of **2** after rapid cooling to 80 K followed by slow warming to 300 K (●). The HS molar fraction as deduced from SQUID measurements after slowly cooling and warming the sample over the temperature range 300 to 50 K is shown for comparison (○ curves). The line is a guide to the eyes and the arrows indicate the broad hysteresis loop.

Three RC experiments to 80 K were successively performed on the same sample and ^{57}Fe Mössbauer experiments were recorded at the same set of temperatures on slow warming to 300 K. The Mössbauer parameters are gathered in Table 1. Figure 11 shows the HS molar fraction

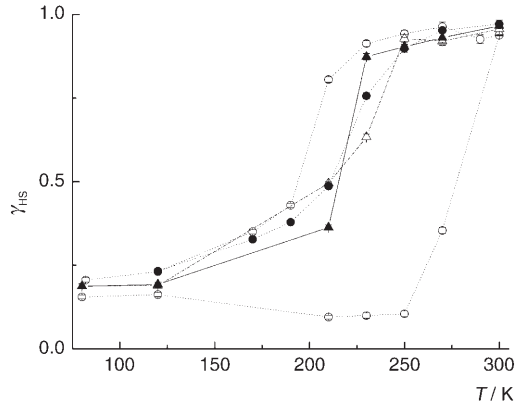

Figure 11. Temperature dependence of the molar fraction of HS molecules, γ_{HS}, for **2** as deduced from ^{57}Fe Mössbauer spectroscopy, after rapid cooling to 80 K followed by slow warming and cooling over the temperature range 80–300 K. The γ_{HS} for the second and third warming modes subsequent to rapid cooling to 80 K is also shown. The symbols (◇), (▲) and (△) refer to the first, second, and third rapid cooling experiments, respectively.

derived from these experiments. At 125 K, the compound is mostly in the LS state. Upon warming to 210 K and above, the HS molar fraction increases to indicate an LS→HS transition curve, which corresponds to that obtained without rapid cooling. The reproducibility of this curve was obtained in the second and third RC experiments. Thus, trapping of the LS state was not reproducible on the same cycled sample.

We prepared $[Fe(NH_2trz)_3]SnF_6 \cdot 1.5\,H_2O$ (**4**) with a different preparation mode compared with **2** to test whether the synthesis pathway could play a role in the observed trapped LS state. For this purpose, we carried out the synthesis in a different solvent (DMF) and did not perform any annealing process during preparation. As a result, the hydration degree was varied and no DMF was inserted, as suggested by the absence of any characteristic peak in the IR spectrum of **4**. The sample was rapidly cooled to 80 K and studied by ^{57}Fe Mössbauer spectroscopy in a similar manner to compound **2**. Full details of the Mössbauer parameters are given in Table 4. The HS molar fraction derived from these experiments is shown in Figure 12. At 80 K and up to 210 K, the compound is mostly in the LS state, ≈20% of Fe^{II} ions stay in the HS state as found for **2**. Upon further warming, an LS→HS transition is observed at $T_{1/2}\uparrow = 274$ K. On slow cooling and warming, a SCO curve with $T_{1/2}\downarrow = 218$ K and $T_{1/2}\uparrow = 248$ K is delineated. This latter SCO may well correspond to the ST curve of **4** in the absence of the RC procedure. Therefore, reproducibility of the trapping of a metastable LS state in a material of this family prepared in a different manner than **2** has been demonstrated.

Table 4. Overview of the ^{57}Fe Mössbauer parameters for **4**.

T [K]	δ[a] [mm s^{-1}]	ΔE_Q[b] [mm s^{-1}]	Γ[c] [mm s^{-1}]	Relative area [%]	Sites
80–98[d]	–	–	–	19.9(6)	HS
	–	–	–	80.1(4)	LS
120↑	1.15(2)	3.34(1)	0.28(1)	20.1(1)	HS
	0.52(1)	0.3[d]	0.26(2)	79.9(6)	LS
210↑	1.10(1)	3.11(1)	0.30(1)	21.3(7)	HS
	0.48(1)	0.26(1)	0.26(1)	78.7(4)	LS
230↑	1.09(1)	3.05(1)	0.30(1)	24.8(1)	HS
	0.47(2)	0.25(1)	0.26(2)	75.2(8)	LS
250↑	1.08(2)	2.97(1)	0.28(1)	39.6(7)	HS
	0.46(1)	0.24(2)	0.24(1)	60.4(5)	LS
270↑	1.07(3)	2.88(1)	0.28(1)	52(1)	HS
	0.45(3)	0.23(1)	0.24(1)	48(1)	LS
300	1.05(2)	2.77(2)	0.26(1)	96(1)	HS
	0.34(1)	0	0.6(4)	4(1)	LS
270↓	1.07(1)	2.88(2)	0.26(1)	95(1)	HS
	0.38(4)	0.1(7)	0.58(1)	5(1)	LS
250↓	1.08(2)	2.97(4)	0.26(1)	92.3(2)	HS
	0.47(2)	0.21(4)	0.22(1)	7.7(1)	LS
230↓	1.09(1)	3.04(2)	0.28(1)	72.1(8)	HS
	0.47(3)	0.24(5)	0.26(1)	27.9(6)	LS
210↓	1.10(2)	3.11(4)	0.28(1)	54.9(1)	HS
	0.48(3)	0.25(4)	0.26(1)	45.1(7)	LS
190↓	1.11(2)	3.16(4)	0.28(1)	36(1)	HS
	0.49(1)	0.26(2)	0.26(1)	64(1)	LS
170↓	1.13(4)	3.22(1)	0.26(1)	30.4(1)	HS
	0.50(2)	0.27(3)	0.26(1)	69.6(7)	LS
84↓	1.16(2)	3.37(1)	0.30(1)	18.2(8)	HS
	0.52(1)	0.29(2)	0.26(1)	81.8(5)	LS
120↑	1.15(3)	3.33(1)	0.30(1)	21.2(6)	HS
	0.52(1)	0.28(1)	0.26(1)	78.8(4)	LS
150↑	1.14(1)	1.14(1)	0.28(1)	25.3(1)	HS
	0.51(1)	0.51(1)	0.26(1)	74.7(6)	LS
170↑	1.12(2)	3.21(1)	0.28(1)	29.4(6)	HS
	0.50(1)	0.27(2)	0.26(1)	70.6(4)	LS
190↑	1.11(1)	3.16(3)	0.28(1)	32.2(4)	HS
	0.50(1)	0.26(1)	0.26(1)	67.7(2)	LS
210↑	1.10(2)	3.10(1)	0.28(1)	37.1(5)	HS
	0.48(1)	0.26(2)	0.26(1)	62.9(4)	LS
230↑	1.10(1)	3.04(1)	0.28(1)	46.9(1)	HS
	0.47(3)	0.24(1)	0.26(1)	53.1(8)	LS
250↑	1.08(1)	2.96(1)	0.28(1)	63.2(8)	HS
	0.46(2)	0.23(2)	0.24(1)	36.8(6)	LS
270↑	1.07(1)	2.87(2)	0.26(1)	79(1)	HS
	0.45(1)	0.22(1)	0.24(1)	21(1)	LS
300	1.05(1)	2.76(2)	0.26(1)	97.7(1)	HS
	0.3(1)	0.1(2)	0.28(4)	2.3(2)	LS

[a] δ = isomer shift relative to α-iron. [b] ΔE_Q = quadrupole splitting. [c] Γ = width at half maximum. [d] after rapid cooling.

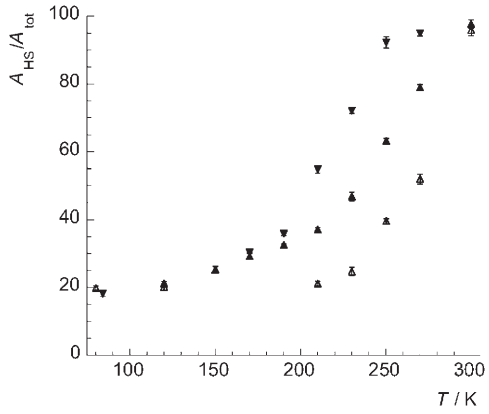

Figure 12. Temperature dependence of A_{HS}/A_{tot} of **4** as deduced from ^{57}Fe Mössbauer spectroscopy. The sample was studied on slow warming (△) and cooling (▼) over the temperature range 80–300 K after being rapidly cooled to 80 K. It was then slowly warmed to 300 K (▲).

SQUID magnetometry: The temperature dependence of the magnetic properties of **2** was reinvestigated on a fresh sample by slowly cooling and warming in the temperature range 300 to 50 K. The susceptibility was measured every 2 K in both temperature modes and care was taken not to overheat the sample above 300 K to avoid any solvent removal (Figure 13) The magnetisation data were converted to a γ_{HS} curve by means of Equation (1):

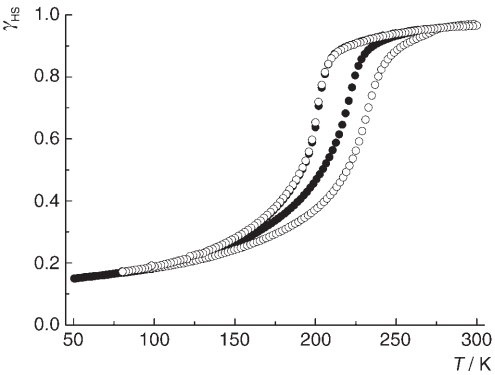

Figure 13. Temperature dependence of the HS molar fraction as deduced from a SQUID measurement of **2** after a) slowly cooling and warming over the temperature range 300–50 K (●) and b) rapid cooling to 80 K followed by slow warming and cooling over the temperature range 80–300 K (○).

$$\gamma_{HS} = \frac{\chi_M T - \chi_M^{LS}(T)}{\chi_M^{HS}(T) - \chi_M^{LS}(T)}$$

in which $\chi_M^{LS}(T) = 184 \times 10^{-6}\,cm^3\,mol^{-1}$ below 50 K and $\chi_M^{HS}(T) = 0.966\,cm^3\,mol^{-1}$ because it follows a Curie law in the HS state.

A spin-transition curve was thus delineated and the transition temperatures determined to be $T_{1/2}\downarrow = 200$ K and $T_{1/2}\uparrow = 218$ K were in perfect agreement with the magnetic data of Figure 3. The sample was subsequently rapidly cooled to 80 K within the SQUID cavity and slowly warmed to 300 K, then slowly cooled to 80 K. For comparison, the susceptibility was also measured every 2 K. Mössbauer spectroscopy of the same sample showed that $T_{1/2}\downarrow$ is preserved, but here $T_{1/2}\uparrow$ increases to 231 K, thus revealing an increase in the hysteresis width by 31 K. The width is lower than that obtained by Mössbauer measurements ($\approx$82 K) because relaxation back to the HS state occurs more rapidly owing to the scanning mode used to record the SQUID data. These experiments thus confirm the reproducibility of the observed effect by Mössbauer spectroscopy on a fresh sample.

X-ray powder diffraction: An X-ray diffraction pattern of **2** was recorded after rapidly cooling the sample to 100 K. Comparison of the powder diffractograms at 100 K before and after RC did not reveal a major difference (Figure 14). In particular, no significant broadening of the lines was observed, which suggests the absence of a crystallographic phase transition for the defect structure.

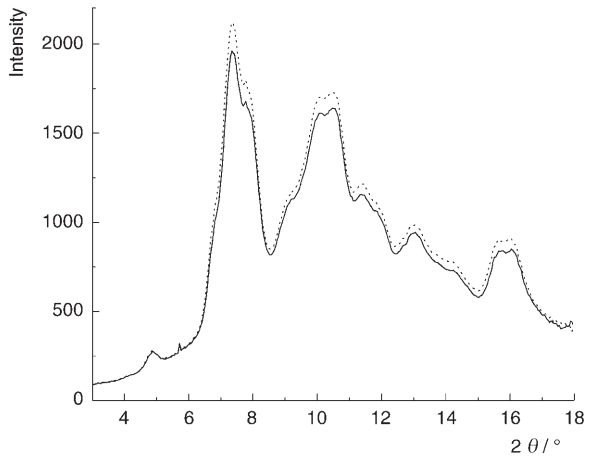

Figure 14. X-ray diffraction patterns of **2** at 100 K after a) slow cooling from 300 K (-----) and b) rapid cooling to 100 K (——). The data were recorded without a detector offset.

Discussion

The origin of the hysteretic magnetic behaviour of 1D 1,2,4-triazole Fe^{II} chain compounds is still being debated.[5] In addition to short-range interactions promoted by the triazoles linking the Fe^{II} ions, hydrogen-bonding and anion–cation interactions are believed to play a decisive role in the cooperative effects associated with the spin transition. Such long-range interactions could be mediated by lattice solvent molecules, non-coordinated counteranions or hydrogen bonding through the substituent of the triazole ligand.[5] Direct hydrogen bonding between chains through the non-coordinated tetrafluoroborato anion (B–F···H) were deduced from WAXS experiments for the ST material $[Fe(Htrz)_2trz](BF_4)$, which displays a broad hysteresis effect.[20] Hydrogen bonding involving the anion was also suggested from recent muon spin-relaxation experiments performed on the ST chain compound $[Fe(NH_2trz)_3](NO_3)_2$, which also displays a broad hysteresis loop.[43] Hydrogen bonding between linear chains through the hydroxyl group of the triazole substituent were observed in the crystal structure of $[Cu(hyptrz)_3]$(4-chloro-3-nitrophenylsulfonate)$_2$·H_2O (hyptrz = 4-(3′-hydroxypropyl)-1,2,4-triazole), a configuration that was also thought to be present in the related Fe^{II} analogue, which displays a cooperative ST with a hysteresis loop of $\approx$50 K.[9f]

In this work, we have incorporated an internal probe into the crystal lattice of $[Fe(NH_2trz)_3]^{2+}$, without modifying the chemical nature of the chains, to study the role of lattice dynamics and supramolecular interactions in 1D chain compounds. We thus directed our choice to a non-coordinated counteranion and focused on the hexafluorostannate metal salt. Indeed, this salt is not only a precursor for the synthesis of new molecular compounds, but it also offers the possibility of using the SnF_6^{2-} anion as a ^{119}Sn Mössbauer probe to study the local surroundings in the crystal lattice of 1D chains. It would thus provide relevant information on local distortions that could be modified by a phase transition and could also probe hydrogen-bonding interactions involving the fluorine atoms.

We successfully prepared new 1D NH_2trz ST compounds with different degrees of hydration incorporating this novel anion as a non-coordinated counteranion, as suggested from IR spectroscopy recorded at room temperature. Monohydrate **1** shows a reversible abrupt ST around 190 K, which is not complete, but accompanied by a hysteresis loop that is $\approx$7 K wide. The ST of hemihydrate **2** has a similar character and is shifted upwards to higher temperatures with a hysteresis loop that is $\approx$16 K wide. The ST of dehydrated **3**, which retains its shape, is shifted downwards and has a hysteresis that is $\approx$13 K wide. The effect of solvent molecules on the mechanism and the spin state is hard to predict;[45] however, several trends were deduced for 1D 1,2,4-triazole chain materials. It is generally accepted that stabilisation of the LS state occurs upon increasing the number of water molecules,[30] and this observation has been found in many other types of SCO compounds. However, stabilisation of the HS state was also encountered.[29] In another case, removing non-coordinated water molecules can even prevent SCO occurring.[9f] Here, varying the water content has an effect on the crystal field because the ST is shifted either upwards or downwards, but no affect is seen on the shape of the ST, which is fully preserved. Such non-coordinated water molecules are expected to be located in the third co-

ordination sphere[9c] and bound to the amino group of the triazole of the chains by hydrogen bonding.[11] Hydrogen bonding to the triazole seems reasonable because the ligand field is only modified by water removal. Also, ^{119}Sn Mössbauer has suggested that the anion is not hydrogen bonded to water molecules. We can thus conclude that non-coordinated water molecules play no role in the cooperative nature of the ST of these compounds and that varying the strength of the supramolecular network involving such species does not affect the cooperative nature of the spin transition.

We have also found that the non-coordinated anion, which is found between the chains, is able to feel the ST of individual chains. This behaviour was suggested primarily on the basis of the evolution of its local distortion registered by ^{119}Sn Mössbauer spectroscopy. Indeed, the SnF_6^{2-} octahedron is found to be regular in the HS state and distorted in the LS state, which presumes that the lattice change associated with the spin-state change of Fe^{II} ions along the chains influences the local distortion of the anion. Also, Mössbauer resonance dramatically varies on crossing the ST range, which is a clear signature of a phase transition (Figure 9). This behaviour may reflect the sensing of long-range elastic interactions between chains associated with ST through the phonons. This result constitutes the second example of ST sensing through the non-coordinated anion and the very first example obtained by Mössbauer spectroscopy. Indeed, a similar conclusion was drawn by following the B–F vibration of the tetrafluoroborato anion in the course of the ST of $[Fe(ptz)_6](BF_4)_2$ (ptz = 1-propyl-tetrazole) by IR spectroscopy.[46] It would also be interesting to complete the Mössbauer results by recording IR spectra for **2** on cooling. The current investigation is also the first combined ^{119}Sn and ^{57}Fe study in an Fe^{II} ST molecular compound. Indeed, to the best of our knowledge, there is only one series of materials on which a combined Mössbauer study could be feasible, namely, the thiospinels $M_2FeSn_3S_8$ (M^+ = Cu, Ag) that were reported to exhibit a HS↔LS spin equilibrium at $T_{1/2} \approx 200$ K, as deduced from magnetic susceptibility and ^{57}Fe Mössbauer spectroscopy measurements.[47] The rigid lattice of this solid-state compound should allow a variable-temperature ^{119}Sn Mössbauer study and provide insights into the spin conversion of these solid-state materials.

The importance of lattice effects on the magnetic properties of SCO complexes is increasingly recognised. These effects were probed by trapping, partially or totally, the metastable HS state by RC for numerous Fe^{II} SCO complexes[48–57] and a few Fe^{III} compounds.[58] Such thermal trapping experiments were attempted to sense cooperative effects of the SCO by looking at the shape of the time dependency of the γ_{HS} relaxation curves at selected temperatures. These experiments were paralleled by thermal relaxation experiments after trapping the HS state by light irradiation (light-induced excited-spin-state trapping (LIESST)).[3] Thermal trapping experiments of the HS state often foreshadow the presence of a LIESST effect, although one example is known to behave differently.[59] Indeed, RC experiments were performed to prevent a structural phase transition and provide insight into the origin of the SCO cooperative behaviour of $[Fe(ptz)_6](BF_4)_2$ that nevertheless displays the LIESST effect. Indeed, on slow cooling and warming the sample from 300 K, an asymmetric hysteretic ST of ≈ 7 K wide is observed.[46] The ST is accompanied by a structural phase transition from $R\bar{3}$ in the HS phase to a disordered structure in the LS phase, as deduced from powder diffraction experiments.[60] The structural phase transition and the hysteresis loop are fully reproducible by thermal cycling. On rapid cooling of the sample, the formation of the $R\bar{3}$ phase is preserved, but a ST is still observed. Therefore, this experiment could nicely demonstrate that the ST has its "own life" and is not dependent on the presence of a crystallographic phase transition.

In the present work, a hysteresis broadening was observed by RC of **2** from 16 to ≈ 82 K (Figure 10). This behaviour is unprecedented because RC allows the trapping of an LS state that is preserved over a temperature range that extends far above the transition temperature on warming, contrary to all reported examples. The LS Fe^{II} ions are believed to be in a metastable state and thermal relaxation back to the stable HS state is expected to occur in an abrupt fashion, which is nicely observed at ≈ 278 K (Figure 10). Upon RC the sample does not change $T_{1/2}\uparrow$, but increases $T_{1/2}\downarrow$, thus revealing a very broad hysteresis loop that is ≈ 82 K wide around the room temperature region. This behaviour cannot be explained by breaking up of crystallites upon RC because such a phenomenon would increase the residual HS fraction at lower temperatures as a result of the creation of defects in the lattice.[3c] On the contrary, no increase in the HS population was observed. The presence of a space group change on RC can also be excluded (Figure 14). We suggest that above ≈ 250 K, thermal relaxation of the frozen distorted form of the SnF_6^{2-} anion towards a regular configuration is observed, and that this relaxation results in SCO behaviour. ^{119}Sn Mössbauer spectroscopy recorded after RC over the temperature range 80 to 300 K would be quite informative and would confirm these hypotheses and should therefore be considered for future investigations.

Interestingly, after thermal relaxation to the stable HS state, the metastable LS state cannot be obtained again after successive RC experiments (Figure 11). The trapping experiments are, however, perfectly reproducible on fresh samples, as shown by SQUID measurements (Figure 13). The immediate non-reproducibility of LS-state trapping may result from the RC experiment itself. Indeed, the strains induced in the lattice by trapping the anion in a distorted state over a wider temperature range and also by its release to reach a regular state may induce local defects that prevent the possibility of trapping the distorted state again. However, time-dependent lattice relaxation should not be excluded; it was not investigated in the present work. We also exclude the possibility that the annealing process undertaken to prepare **2** affected the probability of trapping the metastable LS state because successful RC experiments could be reproduced on **4**, which was not thermo-treated, at high temperatures (Figure 12).

A few examples of Fe^{II} SCO materials are known to present order–disorder transitions of the counteranion.[61–65] Such transitions, which were detected by DSC or μSR, are generally decoupled from the electronic transition. The control of such transitions was recently proposed as a useful tool for the elaboration of a new range of molecular switches for memory or sensing applications.[66] In this case, such an order–disorder of the SnF_6^{2-} anion may be present, but if so, it would be strongly coupled to the SCO because DSC provided the signature of a single-phase transition occurring in the temperature range of the spin transition (Figure 6). Indeed, there is no link between the local distortion of an octahedron and its disorder state because an anion may be distorted/regular and ordered/disordered. For RC, we suggest decoupling the phase transition associated with the anion (whatever its nature) from the electronic transition, a phenomenon resulting in the unusual hysteresis loop widening observed in this work.

Conclusion

An SnF_6^{2-} ion has been successfully inserted in Fe^{II}–1,2,4-triazole 1D SCO chain complexes to probe the local anionic surroundings in their crystal lattice by ^{119}Sn Mössbauer spectroscopy. This dianion is used as a tool to sense the electronic transition occurring in **2** as seen from the modification of its local geometry from a regular form in the HS state to a distorted one in the LS state. By rapidly cooling the sample, followed by a slow warming mode, the distorted form of the anion is assumed to be frozen, which results in the observation of the LS state at temperatures well above $T_{1/2}\uparrow$,[67] and is followed by an abrupt LS→HS crossover that presumably results from thermal relaxation to a regular anionic form. In this respect, the shift of the ST range could presumably be explained by a decoupling process between the electronic SCO and the phase transition of the anion. This phenomenon results in the observation of a broad hysteresis loop around room temperature that is appealing in terms of potential applications. Indeed, taking into account that on cooling, not only the spin state changes from a paramagnetic to a diamagnetic configuration, but also the colour changes from white to purple, there should be some potential applications for these materials. A large temperature variation resulting in the appearance of a LS signal at temperatures at which it should not be observed may be easily detected, for example, by an optical sensor incorporated in an alert device. This property could be useful for the detection of any unwanted temperature exposure in the frame of cold channel applications, for example, for the storage of certain classes of pharmaceutical products (vaccines, medicines and chemicals) that must not be cooled below a certain temperature during shipment and storage. This property could also be useful for direct applications control in industry. The one-shot observation of the hysteresis loop offers the possibility of control to the user and may also find future applications in the fight against forgery. Another perspective is the possibility of addressing the spin state of these compounds by light within their instability domain. Such experiments could provide useful insights into the cooperative mechanisms effective in these materials.

Experimental Section

General: All reagents and solvents were used as received from commercial sources (ACROS) except $[Fe(H_2O)_6]SnF_6$, which was kindly supplied by Prof. G. Levchenko, Donetsk Physical Technical Institute (Ukraine) and whose hydration degree was checked by thermogravimetric measurements. A Heraeus VTR 5036 oven was used for the annealing experiments. CHN analyses were performed by the Zentrale Analytik of the Institut für Organische Chemie (University of Mainz) and at University College London (UK). IR spectra were recorded as KBr pellets by using a BioRad FTS-135 spectrometer. Thermogravimetric analyses (TGA) were performed in air (100 mL min^{-1}) at a heating rate of 1 °C min^{-1} by using a Mettler Toledo TGA/SDTA 851e analyzer. Diffuse reflectance spectra on solids were recorded by using a CARY 5E spectrophotometer with polytetrafluoroethylene as a reference.

$[Fe(NH_2trz)_3]SnF_6 \cdot H_2O$ (1): $[Fe(H_2O)_6](SnF_6)$ (1.59 g, 4 mmol) and ascorbic acid (2 mg) were heated to 65 °C in methanol (10 mL) under a nitrogen atmosphere. The resulting pink solution was filtered and added to a warm solution of NH_2trz (1.4 g, 16.6 mmol) in methanol (10 mL). A white precipitate was instantaneously observed. The mixture was stirred at room temperature for a few hours under a nitrogen atmosphere. The precipitate was filtered, washed with methanol, and dried in air to give **1** as a white powder with slightly pinkish glints (1.43 g, 64 %). IR (KBr): $\tilde{\nu}$ = 3313 (s; ν(H_2O)), 3228 (s; ν(NH_2)), 3114 (s; ν(NH_2)), 3002 (m; ν(CH)), 1634 (s; δ(NH_2)), 1544 (m; $\nu_{1\,ring}$), 1472 (w; $\nu_{2\,ring}$), 1392 (m; $\nu_{3\,ring}$), 1218 (s; ν(N−NH_2)), 1091 (s; δ(C-H)), 1025 (s; $\nu_{6\,ring}$), 997 (s; $\nu_{7\,ring}$), 883 (w; γ(CH)), 624 (vs; ν(C–H ring torsion)), 555 cm^{-1} (vs; ν_3(Sn–F)); UV/Vis (PTFE): λ_{max} = 838 nm ($^5E \leftarrow {}^5T_2$); elemental analysis calcd (%) for $FeC_6H_{14}N_{12}OSnF_6$: C 12.90, H 2.53, N 30.08; found: C 13.52, H 2.52, N 30.15.

$[Fe(NH_2trz)_3]SnF_6 \cdot 0.5\,H_2O$ (2): A similar synthesis to that of **1** was used to give a slightly pink powder that was dried under vacuum in an oven at 50 °C for 30 min. After 15 min, the powder was gently ground. This process led to the formation of a white powder whose hydration degree was confirmed by TGA analyses. IR (KBr): $\tilde{\nu}$ = 3321 (s; ν(H_2O)), 3230 (s; ν(NH_2)), 3114 (s; ν(NH_2)), 3000 (w; ν(CH)), 1634 (s; δ(NH_2)), 1548 (m; $\nu_{1\,ring}$), 1429 (m; $\nu_{2\,ring}$), 1392 (m; $\nu_{3\,ring}$), 1218 (s; ν(N–NH_2)), 1091 (s; δ(C–H)), 1027 (s; $\nu_{6\,ring}$), 997 (s; $\nu_{7\,ring}$), 883 (w; γ(CH)), 624 (vs; ν(C–H ring torsion)), 555 cm^{-1} (vs; ν_3(Sn–F)); UV/Vis (PTFE): λ_{max} = 838 nm ($^5E \leftarrow {}^5T_2$).

$[Fe(NH_2trz)_3]SnF_6 \cdot 1.5\,H_2O$ (4): $[Fe(H_2O)_6](SnF_6)$ (1.6 g, 4 mmol) and ascorbic acid (2 mg) were heated to 65 °C in DMF (10 mL) to give a red solution under a nitrogen atmosphere. Some drops of water were added to the solution and it turned yellow. The solution was filtered and a warm yellow solution of NH_2trz (1.4 g, 16.6 mmol) in DMF (10 mL) was added. A white precipitate was observed and the mixture was stirred at room temperature for one day under a nitrogen atmosphere. The white precipitate was filtered and dried in air (1.62 g, 71 %). IR (KBr): $\tilde{\nu}$ = 3317 (s; ν(H_2O)), 3329 (s; ν(NH_2)), 3115 (s; ν(NH_2)), 2998 (m; ν(CH)), 1654 (s; δ(NH_2)), 1548 (m; $\nu_{1\,ring}$), 1472 (vw; $\nu_{2\,ring}$), 1392 (m; $\nu_{3\,ring}$), 1218 (s; ν(N–NH_2)), 1090 (s; δ(C–H)), 1027 (s; $\nu_{6\,ring}$), 996 (s; $\nu_{7\,ring}$), 912 (w; γ(CH)), 624 (vs; ν(C–H ring torsion)), 555 cm^{-1} (vs; ν_3(Sn–F)); UV/Vis (PTFE): λ_{max} = 855 nm ($^5E \leftarrow {}^5T_2$); elemental analysis calcd (%) for $FeC_6H_{15}N_{12}O_{1.5}SnF_6$: C 12.87, H 2.7, N 30.03; found: C 13.27, H 2.29, N 29.82.

Study of the spin transition: Magnetic susceptibilities were measured at 1.8 to 300 K with a Quantum Design MPMS2 SQUID magnetometer equipped with a 5.5 T magnet operating at 1 T. The samples were inserted into gelatine capsules and mounted on a plastic straw. The magnetic data were corrected for diamagnetic contributions, which were estimated

from Pascal's constants. For the RC experiment, the plastic straw containing the sample was immersed in liquid nitrogen, and then quickly inserted into the magnetometer, which was tempered at 80 K. ^{57}Fe Mössbauer spectra were recorded at various temperatures between 80 and 300 K in transmission geometry by using a conventional constant acceleration spectrometer with a nitrogen cryostat. The source of ^{57}Co(Rh) was kept at RT. The samples were sealed in a Plexiglas sample holder. The spectra were fitted to Lorentzian curves by using Recoil 1.03a Mössbauer Analysis Software[68] assuming equal Debye–Waller factors of the HS and LS states of the Fe^{II} ions. Isomer shifts refer to α-Fe at RT. For the RC experiments, the extremity of the sample rod was rapidly immersed into a Dewar filled with liquid nitrogen. The sample rod was then quickly inserted into the cryostat and a Mössbauer spectrum was recorded at 80 K. Mössbauer spectra at selected temperatures were then recorded on slow warming and cooling over the temperature range 80 to 300 K. ^{119}Sn Mössbauer measurements were measured in transmission geometry by using a ^{119m}Sn ($CaSnO_3$) source operating at RT. Spectra were recorded on cooling by using a cryostat operating over the range 300 to 4.2 K. All isomer shifts refer to $CaSnO_3$. DSC measurements were carried out under a helium atmosphere by using a Perkin–Elmer DSC Pyris 1 instrument equipped with a cryostat and operating down to 98 K. Aluminium capsules were loaded with 14 to 30 mg of the sample and sealed. The heating and cooling rates were fixed at 5 K min^{-1}. Temperatures and enthalpies were calibrated over the temperature range of interest by using the crystal–crystal transitions of pure cyclopentane (≥99 %).

X-ray powder diffraction (XRPD): X-ray powder patterns were recorded at RT from $2\theta = 5$ to 70° with an interval of 0.02° by using a SIEMENS D-5000 counter diffractometer working with $Cu_{K\alpha}$ radiation ($\lambda =$ 1.5418 Å). Temperature-dependent XRPD measurements were performed by using an Oxford Diffraction Xcalibur 2 single-crystal diffractometer equipped with a Cryojet XL cryostat liquid nitrogen blower using $Mo_{K\alpha}$ radiation ($\lambda = 0.71073$ Å). A borosilicate glass capillary 0.3 mm in diameter was filled with the sample. The sample-to-detector distance was 130 mm. To cover a wider range of 2θ, the diffractograms were recorded for two detector positions with an offset of 0 and 12°, respectively. The detector position at $\theta = 12°$ resulted in a systematic distortion of the diffractogram. Correct d values were calculated from a reference mineral (Kyanite) with known peak positions. The acquisition time per sample was 180 s and the sample rotation was 3° s^{-1}. The sample was mounted at RT and slowly cooled to 100 K. In a second run, the sample was slowly warmed from 100 K to RT; 10 min per cooling step were necessary between two measurements. The reading error on the temperature was approximately 1 K. The relative intensity of the HS phase I_{HS}/I_{tot} was obtained by a least-squares refinement to a Gaussian lineshape.[69] For the RC experiments, the sample holder was immersed into a Dewar filled with liquid nitrogen, and then mounted on the diffractometer with the temperature set at 100 K by means of a stream of nitrogen. The mounting procedure took less than one minute. The corresponding data were collected without detector offset.

Acknowledgements

This work was partly funded by the Deutsche Forschungsgemeinschaft (Priority Programme No. 1137), the Fonds Special de Recherche of the Université Catholique de Louvain, the IAP-VI (P6/17) INANOMAT programme, the Fonds der chemischen Industrie and the Fonds National de la Rercherche Scientifique (Crédit aux Chercheurs). We thank L. Marchese for providing access to powder and single-crystal X-ray diffractometers.

[1] E. Breuning, M. Ruben, J.-M. Lehn, F. Renz, Y. Garcia, V. Ksenofontov, P. Gütlich, E. K. Wegelius, K. Rissanen, *Angew. Chem.* **2000**, *112*, 2563; *Angew. Chem. Int. Ed.* **2000**, *39*, 2504.

[2] S. Cobo, G. Molnár, J. A. Real, A. Bousseksou, *Angew. Chem.* **2006**, *118*, 5918; *Angew. Chem. Int. Ed.* **2006**, *45*, 5786.

[3] a) P. Gütlich, A. Hauser, H. Spiering, *Angew. Chem.* **1994**, *106*, 2109; *Angew. Chem. Int. Ed. Engl.* **1994**, *33*, 2024; b) P. Gütlich, Y. Garcia, H. A. Goodwin, *Chem. Soc. Rev.* **2000**, *29*, 419; c) P. Gütlich, Y. Garcia, H. Spiering in *Magnetism: From Molecules to Materials, Vol. IV* (Eds.: J. S. Miller, M. Drillon), Wiley-VCH, Weinheim, **2003**, pp. 271–344.

[4] Spin Crossover in Transition Metal Compounds (Eds.: P. Gütlich, H. A. Goodwin), Springer, Berlin-Heidelberg, **2004**.

[5] Y. Garcia, V. Niel, M. C. Muñoz, J. A. Real, *Top. Curr. Chem.* **2004**, *233*, 229.

[6] a) O. Kahn, J. Kröber, C. Jay, *Adv. Mater.* **1992**, *4*, 718; b) O. Kahn, C. Jay-Martinez, *Science* **1998**, *279*, 44.

[7] Y. Garcia, V. Ksenofontov, P. Gütlich, *Hyperfine Interact.* **2002**, *139/140*, 543.

[8] N. V. Bausk, S. B. Erenburg, L. G. Lavrenova, L. N. Mazalov, *J. Struct. Chem.* **1994**, *35*, 509.

[9] a) A. Michalowicz, J. Moscovici, B. Ducourant, D. Cracco, O. Kahn, *Chem. Mater.* **1995**, *7*, 1833; b) A. Michalowicz, J. Moscovici, O. Kahn, *J Phys IV* **1997**, *7*, 633; c) Y. Garcia, P. J. van Koningsbruggen, G. Bravic, P. Guionneau, D. Chasseau, G. L. Cascarano, J. Moscovici, K. Lambert, A. Michalowicz, O. Kahn, *Inorg. Chem.* **1997**, *36*, 6357; d) A. Michalowicz, J. Moscovici, Y. Garcia, O. Kahn, *J. Synchrotron Radiat.* **1999**, *6*, 231; e) A. Michalowicz, J. Moscovici, J. Charton, F. Sandid, F. Benamrane, Y. Garcia, *J. Synchrotron Radiat.* **2001**, *8*, 701; f) Y. Garcia, J. Moscovici, A. Michalowicz, V. Ksenofontov, G. Levchenko, G. Bravic, D. Chasseau, P. Gütlich, *Chem. Eur. J.* **2002**, *8*, 4992.

[10] T. Yokoyama, Y. Murakami, M. Kiguchi, T. Komatsu, N. Kojima, *Phys Rev B* **1998**, *58*, 14238.

[11] K. Drabent, Z. Ciunik, *Chem. Commun.* **2001**, 1254.

[12] Y. Garcia, P. J. van Koningsbruggen, G. Bravic, D. Chasseau, O. Kahn, *Eur. J. Inorg. Chem.* **2003**, 356.

[13] G. Schwarzenbacher, M. S. Gangl, M. Goriup, M. Winter, M. Grunert, F. Renz, W. Linert, R. Saf, *Monatsh. Chem.* **2001**, *132*, 519.

[14] T. Fujigaya, D.-L. Jiang, T. Aida, *J. Am. Chem. Soc.* **2005**, *127*, 5484.

[15] a) M. Seredyuk, A. B. Gaspar, V. Ksenofontov, S. Reiman, Y. Galyametdinov, W. Haase, E. Rentschler, P. Gütlich, *Hyperfine Interact.* **2006**, *166*, 385; b) M. Seredyuk, A. B. Gaspar, V. Ksenofontov, S. Reiman, Y. Galyametdinov, W. Haase, E. Rentschler, P. Gütlich, *Chem. Mater.* **2006**, *18*, 2513.

[16] J. G. Haasnoot, G. Vos, W. L. Groeneveld, *Z. Naturforsch B* **1977**, *32*, 1421.

[17] J. Kröber, J.-P. Audière, R. Claude, E. Codjovi, O. Kahn, J. G. Haasnoot, F. Grolière, C. Jay, A. Bousseksou, J. Linares, F. Varret, A. Gonthier-Vassal, *Chem. Mater.* **1994**, *6*, 1404.

[18] L. G. Lavrenova, V. N. Ikorskii, V. A. Varnek, I. M. Oglezneva, S. V. Larionov, *Koord. Khim.* **1986**, *12*, 207.

[19] O. Kahn, E. Codjovi, Y. Garcia, P. J. van Koningsbruggen, R. Lapouyade, L. Sommier in *Molecule-based magnetic materials, Vol. 644*, (Eds.: M. M. Turnbull, T. Sugimoto, L. K. Thompson), ACS Symposium Series, Washington, **1996**, Chapter 20, pp. 298–310.

[20] M. Verelst, L. Sommier, P. Lecante, A. Mosset, O. Kahn, *Chem. Mater.* **1998**, *10*, 980.

[21] C. Cantin, J. Kliava, A. Marbeuf, D. Mikaïlitchenko, *Eur. Phys. J. B* **1999**, *12*, 525.

[22] J. Moscovici, A. Michalowicz, *4th TMR-TOSS-Meeting* (Bordeaux, France), **2001**.

[23] L. G. Lavrenova, V. N. Ikorskii, V. A. Varnek, I. M. Oglezneva, S. V. Larionov, *J. Struct. Chem.* **1993**, *34*, 960.

[24] a) Y. G. Shvedenkov, V. N. Ikorskii, L. G. Lavrenova, V. A. Drebushchak, N. G. Yudina, *J. Struct. Chem.* **1997**, *38*, 578; b) V. A. Varnek, L. G. Lavrenova, S. A. Gromikov, *J. Struct. Chem.* **1997**, *38*, 585.

[25] V. A. Varnek, L. G. Lavrenova, *J. Struct. Chem.* **1997**, *38*, 850.

[26] C. Cantin, H. Daubric, J. Kliava, Y. Servant, L. Sommier, O. Kahn, *J. Phys. Condens. Matter* **1998**, *10*, 7057.

[27] V. A. Varnek, L. G. Lavrenova, *J. Struct. Chem.* **1995**, *36*, 104.

[28] Y. Garcia, P. J. van Koningsbruggen, R. Lapouyade, L. Rabardel, O. Kahn, M. Wierczorek, R. Bronisz, Z. Ciunik, M. F. Rudolf *C. R. Acad. Sci., Ser. IIc: Chimie* **1998**, 523.

[29] Y. Garcia, P. J. van Koningsbruggen, R. Lapouyade, L. Fournès, L. Rabardel, O. Kahn, V. Ksenofontov, G. Levchenko, P. Gütlich, *Chem. Mater.* **1998**,*10*, 2426.
[30] V. P. Sinditskii, V. I. Sokol, A. E. Fogel'zang, M. D. Dutov, V. V. Serushkin, M. A. Porai-Koshits, B. S. Svetlov, *Zh. Neorg. Khim.* **1987**, *32*, 1950.
[31] P. J. Moehs, H. M. Haendler, *Inorg. Chem.* **1968**, *7*, 2115.
[32] P. J. van Koningsbruggen, Y. Garcia, E. Codjovi, R. Lapouyade, O. Kahn, L. Fournès, L. Rabardel, *J. Mater. Chem.* **1997**, *7*, 2069.
[33] F. W. D. Woodhams, R. A. Howie, O. Knop, *Can. J. Chem.* **1974**, *52*, 1904.
[34] Y. Calage, R. Tortevois, F. Varret, *J. Phys. Chem. Solids* **1990**, *51*, 911.
[35] A. Benghalem, M. Leblanc, Y. Calage, *Acta Crystallogr., Sect. C: Cryst. Struct. Commun.* **1990**, *C46*, 2453.
[36] M. M. Dîrtu, Y. Garcia, M. Nica, A. Rotaru, J. Linares, F. Varret, *Polyhedron* **2007**, *26*, 2259.
[37] G. Vos, R. A. G. de Graaff, J. G. Haasnoot, A. M. van der Kraan, P. de Vaal, J. Reedijk, *Inorg. Chem.* **1984**, *23*, 2905.
[38] J. J. A. Kolnaar, G. van Dijk, H. Kooijman, A. L. Spek, V. G. Ksenofontov, P. Gütlich, J. G. Haasnoot, J. Reedijk, *Inorg. Chem.* **1997**, *36*, 2433.
[39] Y. Garcia, P. Guionneau, G. Bravic, D. Chasseau, J. A. K. Howard, O. Kahn, V. Ksenofontov, S. Reiman, P. Gütlich, *Eur. J. Inorg. Chem.* **2000**, 1531.
[40] a) R. R. Berret, B. W. Fitzsimmons, *J. Chem. Soc., Chem. Commun.* **1966**, 91; b) R. R. Berret, B. W. Fitzsimmons, *J. Chem. Soc. A* **1967**, 525.
[41] M. Thomman, O. Kahn, J. Guilhem, F. Varret, *Inorg. Chem.* **1994**, *33*, 6029.
[42] K. Boukheddaden, F. Varret, *Hyperfine Interact.* **1992**, *72*, 349.
[43] S. Floquet, M.-L. Boillot, E. Rivière, F. Varret, K. Boukhedddaden, D. Morineau, P. Négrier, *New J. Chem.* **2003**, *27*, 341.
[44] Y. Garcia, S. J. Campbell, J. S. Lord, Y. Boland, V. Ksenofontov, P. Gütlich, *J. Phys. Chem. B* **2007**, *111*, 11111.
[45] W. Zhang, F. Zhao, L. Tao, M. Yuan, Z.-M. Wang, S. Gao, *Inorg. Chem.* **2007**, *46*, 2541.
[46] E. W. Müller, J. Ensling, H. Spiering, P. Gütlich, *Inorg. Chem.* **1983**, *22*, 2074.
[47] M. Womes, J.-C. Jumas, J. Olivier-Fourcade, F. Aubertin, U. Gonser, *Chem. Phys. Lett.* **1993**, *201*, 555.
[48] G. Ritter, E. König, W. Irler, H. A. Goodwin, *Inorg. Chem.* **1978**, *17*, 224.
[49] S. M. Nelson, P. D. A. McIlroy, C. S. Stevenson, E. König, G. Ritter, J. Waigel, *J. Chem. Soc. Dalton Trans.* **1986**, 991.
[50] H. A. Goodwin, K. H. Sugiyarto, *Chem. Phys. Lett.* **1987**, *139*, 470.
[51] a) T. Buchen, P. Gütlich, H. A. Goodwin, *Inorg. Chem.* **1994**, *33*, 4573; b) T. Buchen, P. Gütlich, K. H. Sugiyarto, H. A. Goodwin, *Chem. Eur. J.* **1996**, *2*, 1134.
[52] S. Hayami, Y. Maeda, *Inorg. Chim. Acta* **1997**, *255*, 181.
[53] A. F. Stassen, O. Roubeau, I. Ferrero Gramage, J. Linarès, F. Varret, I. Mutikainen, U. Turpeinen, J. G. Haasnoot, J. Reedijk, *Polyhedron* **2001**, *20*, 1699.
[54] Z. Yu, K. Liu, J. Q. Tao, Z. J. Zhong, X. Z. You, G. G. Siu, *Appl. Phys. Lett.* **1999**, *74*, 4029.
[55] O. Roubeau, M. deVos, A. F. Stassen, R. Burriel, J. G. Haasnoot, J. Reedijk, *J. Phys. Chem. Solids* **2003**, *64*, 1003.
[56] A. B. Gaspar, M. C. Muñoz, N. Moliner, V. Ksenofontov, G. Levchenko, P. Gütlich, J. A. Real, *Monatsh. Chem.* **2003**, *134*, 285.
[57] C. M. Grunert, H. A. Goodwin, C. Carbonera, J.-F. Létard, J. Kusz, P. Gütlich, *J. Phys. Chem. B* **2007**, *111*, 6738.
[58] a) Y. Sunatsuki, Y. Ikuta, N. Matsumoto, H. Ohta, M. Kojima, S. Iijima, S. Hayami, Y. Maeda, S. Kaizaki, F. Dahan, J.-P. Tuchagues, *Angew. Chem.* **2003**, *115*, 1652; *Angew. Chem. Int. Ed.* **2003**, *42*, 1614; b) Y. Ikuta, M. Ooidemizu, Y. Yamahata, M. Yamada, S. Osa, N. Matsumoto, S. Ijima, Y. Sunatsuki, M. Kojima, F. Dahan, J.-P. Tuchagues, *Inorg. Chem.* **2003**, *42*, 7001; c) S. Iijima, F. Mizutani, O. Niwa, N. Matsumoto, Y. Sunatsuki, M. Kojima, *Hyperfine Interact.* **2006**, *166*, 397; d) M. Yamada, H. Hagiwara, H. Torigoe, N. Matsumoto, M. Kojima, F. Dahan, J.-P. Tuchagues, N. Re, S. Ijima, *Chem. Eur. J.* **2006**, *12*, 4536.
[59] J. Jung, G. Schmitt, L. Wiehl, A. Hauser, K. Knorr, H. Spiering, P. Gütlich, *Zh. Phys. B* **1996**, *100*, 523.
[60] J. Kusz, P. Gütlich, H. Spiering, *Top. Curr. Chem.* **2004**, *234*, 129.
[61] J. Fleisch, P. Gütlich, K. M. Hasselbach, W. Müller, *Inorg. Chem.* **1976**, *15*, 958.
[62] E. König, G. Ritter, S. K. Kulshrehtha, S. M. Nelson, *Inorg. Chem.* **1982**, *21*, 3022.
[63] J. M. Holland, J. A. McAllister, Z. Lu, C. A. Kilner, M. Thornton-Pett, M. A. Halcrow, *Chem. Commun.* **2001**, 577.
[64] S. J. Campbell, V. Ksenofontov, Y. Garcia, J. S. Lord, Y. Boland, P. Gütlich, *J. Phys. Chem. B* **2003**, *107*, 14289.
[65] N. Ortega-Villar, A. L. Thompson, M. C. Muñoz, V. M. Ugalde-Saldívar, A. E. Goeta, R. Moreno-Esparza, J. A. Real, *Chem. Eur. J.* **2005**, *11*, 5721.
[66] O. Jeannin, R. Clérac, M. Fourmigué, *J. Am. Chem. Soc.* **2006**, 128, 14649.
[67] Determined on warming after slow cooling **2** from 293 K.
[68] K. Lagarec, D. G. Rancourt, Recoil, Mössbauer Spectral Analysis Software for Windows 1.05, Department of Physics, University of Ottawa, Ottawa (Canada), **1998**.
[69] E. König, G. Ritter, W. Irler, H. A. Goodwin, *J. Am. Chem. Soc.* **1980**, *102*, 4681.

Received: August 22, 2007
Published online: March 7, 2008

